

Chern Mott insulators in the band-filling - coupling strength phase diagram of buckled 3d-oxide honeycomb bilayers

David Doennig,¹ Santu Baidya,² Warren E. Pickett,³ and Rossitza Pentcheva^{2,1,*}

¹*Forschungs-Neutronenquelle Heinz Maier-Leibnitz (FRM II),*

Technische Universität München, Lichtenbergstraße 1, 85748 Garching, Germany

²*Department of Physics and Center for Nanointegration Duisburg-Essen (CENIDE),*

University of Duisburg-Essen, Lotharstr. 1, 47057 Duisburg, Germany

³*Department of Physics, University of California Davis, One Shields Avenue, Davis, CA 95616, U.S.A.*

(Dated: January 26, 2016)

Perovskite bilayers with (111)-orientation combine a honeycomb lattice as a key feature with the strongly correlated, multiorbital nature of electrons in transition metal oxides. In a systematic DFT+ U study we establish trends in the evolution of ground states versus band filling in (111)-oriented $(\text{LaXO}_3)_2/(\text{LaAlO}_3)_4$ superlattices, with X spanning the entire 3d transition metal series. The competition between local quasi-cubic and global triangular symmetry triggers unanticipated broken symmetry phases not accessible for the (001)-growth direction, with mechanisms ranging from Jahn-Teller distortions, to charge-, spin-, and orbital-ordering. Introducing spin-orbit coupling (SOC), we establish that in spite of the small SOC expected for 3d ions, the phase diagram of this broad system includes Chern Mott insulating phases for $X=\text{Ti, Mn, Co}$.

PACS numbers: 73.21.Fg, 73.22.Gk, 75.70.Cn

INTRODUCTION

The discovery and investigation of new phases of matter is a major focus of condensed matter physics. Low dimensionality enhances unconventional behavior, and multiorbital active sites introduce additional degrees of freedom, resulting in more complex behavior than can be studied with simple models. Synthesis and characterization of atomically abrupt transition metal oxide (TMO) heterostructures provides such a platform, and several unanticipated functionalities have been discovered and studied, some having the potential to enhance next generation electronics and spintronics devices by controlling charge, spin, orbital, and lattice degrees of freedom at the nanoscale.[1, 2]

The recent focus on perovskite materials with the (001) growth orientation, most prominently the interface between LaAlO_3 and SrTiO_3 (LAO/STO)[3, 4] and nickelate superlattices,[5] is currently extended to the (111) orientation.[6, 7] In the latter, two triangular BO_6 sublattices form a buckled honeycomb lattice, topologically equivalent to graphene. The honeycomb lattice itself introduces exotic possibilities: Haldane obtained a quantum spin Hall (QSH) system without explicit external field,[8] extended by Wright to a *buckled* honeycomb lattice that accommodates a Chern (quantum anomalous Hall [QAH]) insulator state[9] with topologically protected gap states. Inclusion of spin-orbit-coupling (SOC)[10] and strong interactions[11] provided additional evidence for the robustness of QAH possibilities. The lattice models used in these developments are, however, challenging to realize in real materials, and viable Chern insulators remain a much sought goal.

Compared to graphene and common topological insu-

lators (TI), TMOs possess not only larger band gaps, but offer an abundant palette of phases due to several distinctive features: correlated electron behavior causing spin, charge, and orbital instabilities, multi-orbital configurations combined with spin-orbit coupling (SOC), and several more possible complications. Below we demonstrate that the interplay of strong interactions and SOC effects produce specific spin-fermion systems as candidates for QSH or QAH systems in the 3d (111) bilayers with buckled honeycomb lattice.

The idea of constructing a (111) bilayer from perovskite TMO was introduced by Xiao *et al.* for 4d and 5d systems, pointing to possibilities for “interface engineering of QAH effects”.[12] Building on this foundation, Yang *et al.*[13] and Rüegg and Fiete[14] applied a tight-binding (TB) model for $(\text{LaNiO}_3)_2/\text{LAO}$, and demonstrated that in certain ranges of parameters and magnetic order, topological insulating phases can arise from ordering of a complex combination of e_g orbitals.[14]

Complementary to tight-binding models, material-specific density functional theory (DFT) can contribute to fundamental understanding as well as guide the search for actual materials realizations. Besides examples for 5d systems[15], DFT studies including strong local interaction effects (see below) have recently predicted a Dirac Fermi point for $\text{STO}(111)$ [16] and $\text{LaNiO}_3(111)$ bilayers, quantum confined within LAO.[13, 14, 17, 18] In these cases the Dirac point is ‘protected’ by symmetry; sublattice symmetry breaking leads to a gap-opening due to charge, spin, or orbitally ordered states.[16, 18] Below we demonstrate a direct connection between this Dirac point and SOC-generated Chern insulator phases.

To survey the entire band-filling phase diagram and elucidate the underlying *design principles* of function-

alities, QAH and beyond, we have explored systematically the effect of band filling on the electronic ground state in (111)-oriented $(\text{LaXO}_3)_2/(\text{LaAlO}_3)_4$ superlattices, where X spans the range of trivalent $3d$ ions Ti-Cu. Despite the fact that these systems, unlike LAO/STO(111), have nonpolar interfaces (all cations retain X^{3+} configurations), we find that unexpected phases including QAH regimes proliferate. Competition between local pseudocubic symmetry and global trigonal symmetry as well as additional flexibility, provided by the magnetic and spin degrees of freedom of $3d$ ions, lead to a broad array of distinctive broken symmetry ground states, offering a platform to design 2D electronic functionalities.

Chern insulators have so far been sought mainly in magnetically doped TIs[19], or by combining trivial magnetic insulators with a material with large SOC, either in double perovskites[20] or rocksalt compounds[21, 22]. Of the systems we study, two display simultaneous time reversal symmetry breaking and SOC-driven gap opening. We provide the first examples in a solely $3d$ system of Chern insulators with gap sizes large enough to support room-temperature applications.

DFT calculations were performed on (111)-oriented $(\text{LaXO}_3)_2/(\text{LaAlO}_3)_4$ superlattices with $X = 3d$, using the all-electron full-potential linearized augmented-plane-wave (LAPW) method, as implemented in the WIEN2k code [23]. For the exchange-correlation functional we used the generalized gradient approximation (GGA) [24]. Static local electronic correlations were included in the GGA+ U approach [25] with $U = 5$ eV, $J = 0.7$ eV (for all $X = \text{Ti-Cu } 3d$) and $U = 8$ eV (La $4f$), but the results are robust with respect to variation of U in a reasonable range of values. Additional calculations with the modified Becke-Johnson [26] potential support the obtained electronic behavior. The lateral lattice constant is fixed to $a_{\text{LAO}} = 3.79$ Å, corresponding to superlattices grown on a LAO(111) substrate, unless otherwise stated. Octahedral tilts and distortions were fully taken into account when relaxing atomic positions, whether constrained to P321 symmetry or fully released to P1 symmetry. Additionally, the out-of-plane lattice parameter c was optimized for all superlattices. Spin-orbit coupling (SOC) was included in several cases using the second-variational method. The anomalous Hall conductivity (AHC) was calculated using wannier90[27, 28] interfaced with Wien2k[29].

A central aspect in the $(\text{LaXO}_3)_2/(\text{LaAlO}_3)_4$ (111) honeycomb bilayers is their strong deviation from their bulk analogs. Certain recurring features tied to the t_{2g} and e_g distinction can be identified, thus we discuss them separately. For the t_{2g} subshell the dominating feature is a competition between local pseudo-cubic symmetry and the underlying threefold+inversion symmetry (“P321”) of the ideal bilayer. The (111) bilayering reduces the octahedral symmetry to trigonal and splits the t_{2g} orbital

triplet into $a_{1g} + e'_g$. Breaking this symmetry allows occupation of the cubic d_{xy} , d_{yz} , or d_{zx} orbitals.

$X = \text{Ti}^{3+} 3d^1$. The above scenario arises most vividly for the LaTiO_3 bilayer, which displays the richest behavior among the t_{2g} systems. In contrast to bulk LaTiO_3 which is a distorted $Pbnm$, G-type antiferromagnetic (AFM) Mott insulator with $1/\sqrt{3}(d_{xy} + d_{yz} + d_{zx})$ orbital order [30, 31], the ground state at the lateral lattice constant of LaAlO_3 (a_{LAO}) (Fig. 1a) is a ferromagnetic (FM) orbitally ordered Mott insulator, displaying an unusual staggered d_{xz} , d_{yz} occupation and a very narrow (0.2 eV bandwidth) lower Hubbard band. Consistent with this extremely localized character, the corresponding AFM state with the same orbital polarization, shown in Fig. 1e, is only 4 meV/u.c. higher in energy, suggesting a weak exchange coupling of ~ 1 meV.

Constraining to P321 space group with symmetry-equivalent Ti ions results in e'_g orbital polarization. Despite its high energy cost of 0.4 eV/Ti, this state is noteworthy due to the unusual direction reversal of bands in the vicinity of K and K' (Fig. 1f and zoom-in of the band structure in Fig. 1g). This intertwining of bands suggests topological character.

Inclusion of SOC with out-of-plane magnetization leads to a band inversion and gap-opening (green line in Fig. 1g) and a nonzero AHC. The disparity at K and K' signals the loss of equivalence of the two Ti ions, reflected in a surprisingly large orbital moment on only one of the ions: $0.11\mu_B$ versus just $0.01\mu_B$ on the other.

Ti orbital polarization is highly susceptible to strain-tuning: applying tensile strain by imposing the lateral lattice constant of SrTiO_3 tips the pseudo-cubic/trigonal symmetry balance, stabilizing occupation of the a_{1g} orbital (Fig. 1h). The band structure just below the gap is comprised of two filled bands with Dirac crossings at K and K', similar to the LAO/STO(111) case,[18] where the $3d^{0.5}$ band filling fixes the Dirac points at E_F instead.

$X = \text{V}^{3+} 3d^2$. In the LaVO_3 bilayer trigonal symmetry splitting dominates over the pseudocubic crystal field: The AFM ground state, displayed in Fig. 1b, is gapped due to occupation of the majority e'_g doublet. This is insensitive to strain and at variance with the bulk G-type d_{xz} , d_{yz} orbital ordering (d_{xy} is occupied on all sites)[31, 32]. The FM state (Fig. 1c) with the same orbital polarization is 73 meV/u.c. higher in energy. The set of four bands, topologically similar to those of the metastable 2LaTiO_3 case (Fig. 1f), are here entirely filled.

$X = \text{Cr}^{3+} 3d^3$. The Cr bilayer is electronically trivial: a half-filled t_{2g} -band ($t_{2g,\uparrow}^3$, $S = \frac{3}{2}$), thus no orbital degrees of freedom, and antiferromagnetic order (Fig. 1d).

Now we turn to the e_g systems: Consistent with the tight-binding model of Xiao *et al.*[12] a distinctive set of four bands emerges for a FM open e_g subshell: nearly flat bottom and top bands interconnected by two dispersive bands, providing a Dirac point crossing at the K and K'

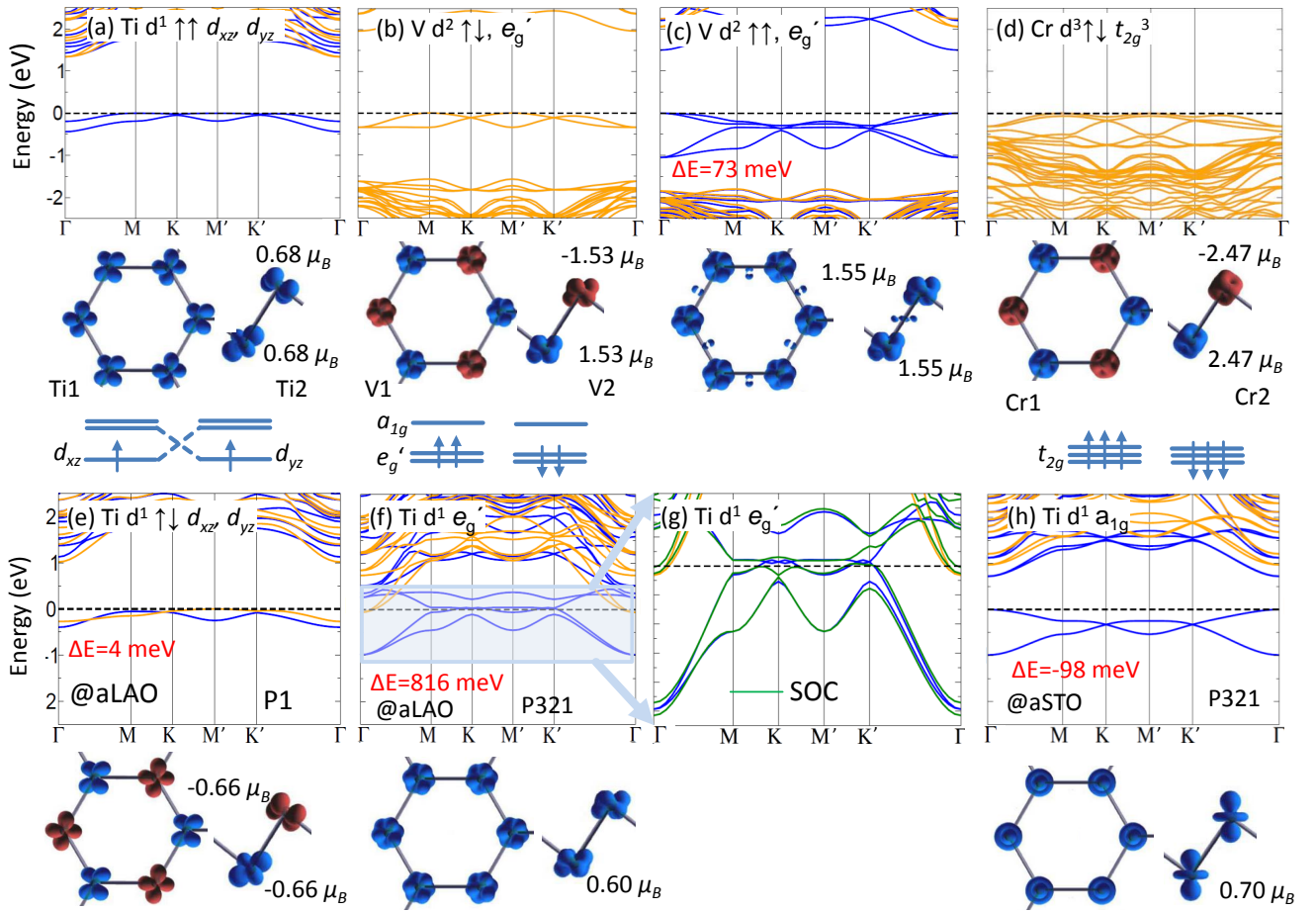


FIG. 1: Electronic ground (a-d) and selected metastable (e-h) states in $(\text{LaXO}_3)_2/(\text{LaAlO}_3)_4(111)$ for t_{2g} systems $X=\text{Ti, V, Cr}$. Shown are the band structures with blue/orange denoting the majority/minority bands, and isosurfaces of the spin density, with majority in blue and minority in red. In cases (a,e,h) the integration range is $E_F-1\text{eV}, E_F$ to emphasize the orbital polarization. Energies of metastable states are provided in red.

points and quadratic contact with the flat bands at the Γ point (cf. Fig. 2a-c,h,l). A key finding is that a pinning of the Dirac point at E_F is not solely determined by band filling, but also by an interplay of orbital and spin degrees of freedom, as proven for the cases of $X=\text{Mn, Co}$ and Ni . Equivalence of the two sublattices again becomes crucial. This symmetry is found to be broken in *all* e_g system ground states where the Dirac point is initially at the Fermi level. We identify distinct origins of symmetry breaking and the resulting gap opening in each system, as discussed below.

$X=\text{Mn}^{3+} 3d^4$. Within P321 symmetry a Dirac-point Fermi surface results (Fig.2a) from the half-filled e_g -band of the high spin Mn ion ($t_{2g,\uparrow}^3 e_{g,\uparrow}^1$). Releasing structural symmetry restrictions leads to a Jahn-Teller (JT) distortion with an elongation of the apical Mn-O bond lengths to 2.07-2.11 Å and variation of the basal distances between 1.89-1.98 Å, associated with alternating $d_{3y^2-r^2}$, $d_{3x^2-r^2}$ occupation on the A and B sublattices (Fig. 2e). This symmetry breaking opens a gap of 0.8 eV and also

lifts the quadratic band touching degeneracy at Γ . The Jahn-Teller distortion is also present in the AFM order (not shown), which is 88 meV/u.c. higher in energy. The significantly flatter bands reflect electronic decoupling of the two sublattices, similar to the AFM LaNiO_3 bilayer, discussed below.

$X=\text{Fe}^{3+} 3d^5$. The ground state of the LaFeO_3 bilayer is a HS AFM band insulator with nearly spherically symmetric charge and spin density on the Fe site, characteristic of a half-filled $3d$ band ($t_{2g,\uparrow}^3 e_{g,\uparrow}^2$ with $S=\frac{5}{2}$, cf. Fig 2d). For comparison, bulk LaFeO_3 is a G-type AFM with orthorhombic $Pnma$ structure.

$X=\text{Co}^{3+} 3d^6$. The LaCoO_3 bilayer exhibits an abundant phase diagram respect to spin degrees of freedom. We note that bulk LaCoO_3 has a low spin (LS) (t_{2g}^6) ground state, but becomes ferromagnetic e.g. as a strained film [33]. Constraining symmetry to P321 renders another case where the Fermi level is pinned at the Dirac point (Fig. 2b) with Co being in the intermediate spin (IS) state ($t_{2g}^5 e_g^1$). Orbital ordering of the e_g elec-

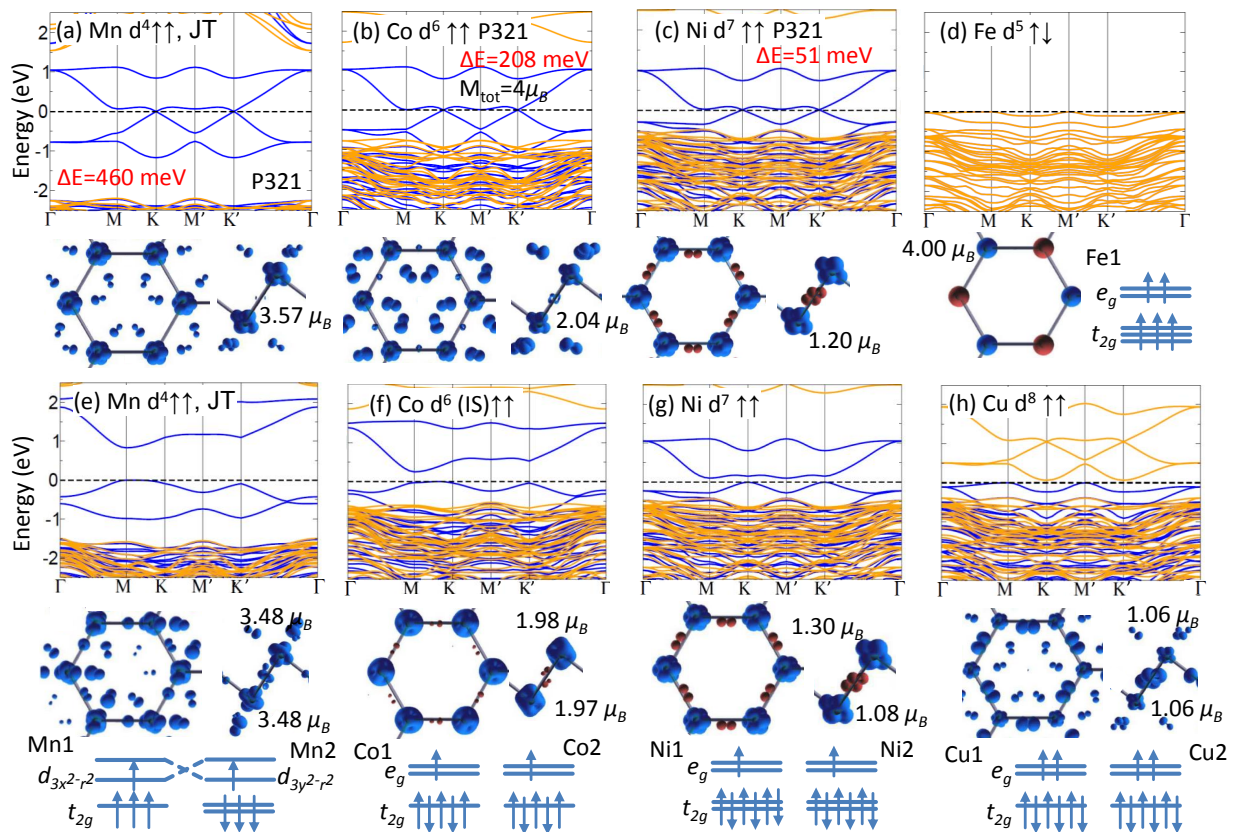


FIG. 2: Presentation as in Fig. 1, but for e_g systems $X=\text{Mn, Fe, Co, Ni, and Cu}$. A striking feature is the similarity in band structure of $X=\text{Mn, Co, Ni}$, despite the formally different band filling: a Dirac point Fermi surface within P321 (a)-(c) and a gap opening due to symmetry breaking.

tron and t_{2g} hole leads to a FM insulator (0.21 eV lower in energy) with a moment of $1.97\mu_B$ (Fig. 2f). A further metastable state, only 19 meV less favorable, exhibits a new type of *spin state symmetry breaking* where the two Co sublattices assume IS and LS states with very flat bands accompanied by a $d_{x^2-y^2}$ orbital occupation on the IS Co sublattice.

$X=\text{Ni}^{3+} 3d^7$. Bulk LaNiO_3 is a $R\bar{3}c$ correlated metal. [30]. Within P321 symmetry a Dirac-point Fermi surface is obtained for the LaNiO_3 bilayer [13, 14, 18] (cf. Fig. 2c). However, breaking the equivalency of the two triangular sublattices opens a gap of 0.25 eV at the Fermi level (cf. Fig. 2g) [18]. Here the mechanism is disproportionation of the Ni sublattice, expressed in different magnetic moments of 1.30 and $1.08\mu_B$. AFM coupling of the two bilayers results in flat bands (not shown here), defining a band gap of ~ 1 eV with orbital polarization at the Ni sites, as recently observed in a NdNiO_3 bilayer. [6] This illustrates how antiferromagnetic order provides the necessary decoupling of the two trigonal bilayers, analogous to the $\text{La}_2\text{NiAlO}_6$ double perovskite where the single triangular Ni-layers are separated by Al-layers [18].

$X=\text{Cu}^{3+} 3d^8$. This case yields a straightforward $e_{g,\uparrow}^2 S=1$ ion at half filling of the e_g bands, where the occupied

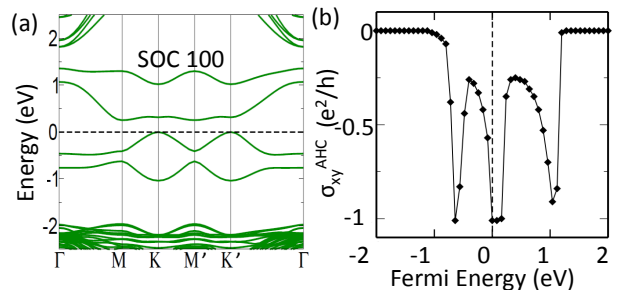


FIG. 3: (a) Effect of SOC on $(\text{LaMnO}_3)_2/(\text{LaAlO}_3)_4$, opening a gap of 0.2 eV for magnetization along [100]. (b) Calculated AHC versus (rigid band) chemical potential in units of (e^2/h) , revealing a Chern number $C=-1$ for this state.

(majority) and unoccupied (minority) set of four bands are separated by a very low energy spin-flip excitation gap (Fig. 2h, see also [12]). Although Cu^{3+} is uncommon (bulk LaCuO_3 is metallic and must be synthesized under pressure), [34] it might be stabilized by non-equilibrium epitaxial synthesis.

Spin-orbit coupling, recognized as important in 4d and 5d materials, introduces new phases in these 3d bilayers.

As mentioned above, SOC leads to a band inversion and gap opening in the P321 $X = \text{Ti}$ bilayer. Unexpectedly strong effects occur for $X = \text{Mn}$ and Co : SOC gaps the Dirac point as well as the quadratic band touching at Γ in each of these systems. $(\text{LaMnO}_3)_2$ shows the strongest influence of SOC, with an in-plane [100] easy axis (Fig. 3(a)); $(\text{LaCoO}_3)_2$ has an out-of plane easy axis. The calculated AHC,[27–29] in Fig. 3(b), reveals $(\text{LaMnO}_3)_2$ with P321 symmetry to be a $C = -1$ Chern insulator with an impressive gap size of 200 meV, large enough to enable room temperature study and applications. Allowing symmetry breaking to P1 symmetry involves geometrical relaxation coupled with orbital rearrangement to the JT ground state in Fig. 2(e). Along this path lies a first order phase transition where SOC entangled bands disentangle as strong interaction takes over; the orbital polarization changes, and the Chern number reverts to zero (trivial insulator). This transition reveals how the direct competition between SOC and strong correlation effects (JT relaxation) determines the ground state even in $3d$ bilayers with purported weak SOC.

Our mapping of the band-filling phase diagram and the prominent effect of SOC establishes that metastable Chern Mott insulator phases lie within the band-filling – interaction strength phase diagram of buckled $3d$ -oxide honeycomb bilayers besides. These topological insulating phases are complemented by a variety of unanticipated ground states, arising from assorted symmetry-breaking forces, offering new possibilities to tailor 2D functionality in oxide materials.

Discussions with Binghai Yan are gratefully acknowledged. This work was partially supported by the German Science Foundation within SFB/TR80, project G3 (to R.P. and D.D.) and by U.S. Department of Energy Grant No. DE-FG02-04ER46111 (to W.E.P.).

* Electronic address: Rossitza.Pentcheva@uni-due.de

- [1] H. Y. Hwang, Y. Iwasa, M. Kawasaki, B. Keimer, N. Nagaosa and Y. Tokura, *Nat. Mater.* **11**, 103 (2012).
- [2] J. Mannhart, and D. G. Schlom, *Science* **327**, 1607 (2010).
- [3] R. Pentcheva, and W. E. Pickett, *J. Phys.: Condens. Matter* **32**, 043001 (2010).
- [4] P. Zubko, S. Gariglio, M. Gabay, P. Ghosez, and J.-M. Triscone, *Annu. Rev. Condens. Matter Phys.* **2**, 141 (2011).
- [5] J. Chaloupka, and G. Khaliullin, *Phys. Rev. Lett.* **100**, 016404 (2008).
- [6] S. Middey, D. Meyers, M. Kareev, E. J. Moon, B. A. Gray, X. Liu, J. W. Freeland and J. Chakhalian, *Appl. Phys. Lett.* **101**, 261602 (2012).
- [7] M. Gibert, P. Zubko, R. Scherwitzl, J.-M. Triscone, *Nat. Mater.* **11**, 195 (2012).
- [8] F. D. M. Haldane, *Phys. Rev. Lett.* **61**, 2015 (1988).
- [9] A. R. Wright, *Sci. Rep.* **3**, 2736 (2013).
- [10] C. L. Kane and E.J. Mele, *Phys. Rev. Lett.* **95**, 226801 (2005).
- [11] S. Raghu, X. L. Qi, C. Honerkamp, and S.-C. Zhang, *Phys. Rev. Lett.* **100**, 156401 (2008).
- [12] D. Xiao, W. Zhu, Y. Ran, N. Nagaosa and S. Okamoto, *Nature Commun.* **2**, 596 (2011).
- [13] K.-Y. Yang, W. Zhu, D. Xiao, S. Okamoto, Z. Wang, and Y. Ran, *Phys. Rev. B* **84**, 201104(R) (2011).
- [14] A. Rüegg, and G. A. Fiete, *Phys. Rev. B* **84**, 201103 (2011).
- [15] J. L. Lado, V. Pardo, and D. Baldomir, *Phys. Rev. B* **88**, 155119 (2013).
- [16] D. Doennig, W. E. Pickett and R. Pentcheva, *Phys. Rev. Lett.* **111**, 126804 (2013).
- [17] A. Rüegg, C. Mitra, A.A. Demkov and G. A. Fiete, *Phys. Rev. B* **85**, 245131 (2012); *ibid.* **88** 115146 (2013).
- [18] D. Doennig, W. E. Pickett, and R. Pentcheva, *Phys. Rev. B* **89**, 121110 (2014).
- [19] C.-Z. Chang, *et al.*, *Science* **340**, 167 (2013).
- [20] A. M. Cook, A. Paramekanti, *Phys. Rev. Lett.* **113**, 077203 (2014).
- [21] K. F. Garrity and D. Vanderbilt, *Phys. Rev. B* **90**, 121103(R) (2014).
- [22] H. Zhang, J. Wang, G. Xu, Y. Xu and S.-C. Zhang, *Phys. Rev. Lett.* **112**, 096804 (2014).
- [23] P. Blaha, K. Schwarz, G. K. H. Madsen, D. Kvasnicka, and J. Luitz, *WIEN2k, An Augmented Plane Wave Plus Local Orbitals Program for Calculating Crystal Properties*, ISBN 3-9501031-1-2 (Vienna University of Technology, Vienna, Austria, 2001).
- [24] J. P. Perdew, K. Burke and M. Ernzerhof, *Phys. Rev. Lett.* **77**, 3865 (1996).
- [25] V. I. Anisimov, J. Zaanen, and O. K. Andersen, *Phys. Rev. B* **44**, 943 (1991).
- [26] F. Tran and P. Blaha, *Phys. Rev. Lett.* **102**, 226401 (2009).
- [27] A. A. Mostofi, J. R. Yates, Y. S. Lee, I. Souza, I. Vanderbilt, N. Marzari, *Comput. Phys. Commun.* **178**, 685 (2008).
- [28] X. Wang, J. R. Yates, I. Souza, D. Vanderbilt, *Phys. Rev. B* **74**, 195118 (2006).
- [29] J. Kuneš, R. Arita, P. Wissgott, A. Toschi, H. Ikeda, K. Held, *Comp. Phys. Commun.* **181**, 1888 (2010).
- [30] T. Arima, Y. Tokura and J. B. Torrance, *Phys. Rev. B* **48**, 17006 (1993).
- [31] E. Pavarini, S. Biermann, A. Poteryaev, A. I. Lichtenstein, A. Georges, and O. K. Andersen, *Phys. Rev. Lett.* **92**, 176403 (2004).
- [32] M. De Raychaudhury, E. Pavarini, O.K. Andersen, *Phys. Rev. Lett.* **99**, 126402 (2007).
- [33] H. Hsu, P. Blaha and R. M. Wentzcovitch, *Phys. Rev. B* **85**, 140404 (2012).
- [34] M. Karppinen, H. Yamauchi, T. Ito, H. Suematsu, O. Fukunaga, *Matl. Sci. & Eng.* **41**, 59 (1996).